Subtidal water level variation controlled by river flow and tides

F. A. Buschman,[1] A. J. F. Hoitink,[1,2] M. van der Vegt,[1] and P. Hoekstra[1]

Received 3 May 2009; revised 28 July 2009; accepted 6 August 2009; published 15 October 2009.

[1] Subtidal water level dynamics in the Berau river, East Kalimantan, Indonesia, feature a pronounced fortnightly variation. The daily mean water levels at a station about 60 km from the sea are 0.2–0.6 m higher during spring tide than during neap tide. To explain the underlying mechanisms, a local subtidal momentum balance is set up from field data, using continuous discharge estimates inferred from measurements taken with a horizontal acoustic Doppler current profiler. It is demonstrated that terms accounting for friction and variation in the water surface gradient are dominant in the subtidal momentum balance. To further investigate the sources of subtidal water level variation, a generic method of analysis is proposed to decompose the subtidal friction term into contributions caused by river flow, by interaction between tidal motions and river flow, and by the tidal motions alone. At the station under study, mainly the river-tide interaction term is responsible for generating fortnightly variation of the subtidal water level. The contribution from interaction between diurnal, semidiurnal, and quarterdiurnal tides to subtidal friction is significantly smaller. Provided that the reduction of tidal velocity amplitudes with increasing discharges can be predicted from a regression model, the results presented herein can be used to predict changes in subtidal water levels as a result of increased river discharges.

Citation: Buschman, F. A., A. J. F. Hoitink, M. van der Vegt, and P. Hoekstra (2009), Subtidal water level variation controlled by river flow and tides, *Water Resour. Res.*, *45*, W10420, doi:10.1029/2009WR008167.

1. Introduction

[2] Historically, the interaction of river flow with tides in lowland rivers has been subject to investigation by oceanographers. In their studies on upriver tidal propagation, the river flow is generally treated as a constant, distorting the propagation of diurnal and semidiurnal tides [e.g., *Dronkers*, 1964; *Godin*, 1991; *Jay*, 1991]. Adopting the perspective of a hydrologist, at first glance tides may seem a periodic perturbation of the river flow. The interactions of tides with the river flow are, however, not all periodic. River-tide interaction creates steady as well as oscillatory gradients of the subtidal (averaged over a diurnal period) water surface, steepening the surface level profile up to the point of extinction of the tide [*LeBlond*, 1979; *Godin and Martínez*, 1994]. In flat areas, the region of influence of a permanent water level gradient and low-frequent surface level variations potentially reaches much further inland than diurnal and semidiurnal tidal motion [*Godin and Martínez*, 1994].

[3] The analysis of subtidal water level variation in response to river discharge waves requires long-term data series of discharge. Obtaining continuous discharge estimates has recently become facilitated by the development of techniques to convert data from horizontally deployed acoustic Doppler current profilers (H-ADCPs) to discharge [*Le Coz et al.*, 2008; *Nihei and Kimizu*, 2008; *Hoitink et al.*, 2009]. This paper provides an investigation of the sources of subtidal water level variation, using continuous series of discharge obtained from an H-ADCP in a relatively pristine tidal river in the tropics. The tidal river dewaters a relatively small catchment with a river discharge that varies, relatively rapidly, around an average of about 600 $m^3 s^{-1}$.

[4] The generation of subtidal water level variation due to river-tide interactions can be captured in analytical one-dimensional models [*LeBlond*, 1979; *Kukulka and Jay*, 2003a; *Jay and Flinchem*, 1997]. In succession to an earlier paper on tidal river hydrodynamics [*LeBlond*, 1978], *LeBlond* [1979] derived subtidal balance equations of mass and momentum. These balances resulted after decomposing the cross-section averaged river velocity into a mean flow contribution, a contribution representing fortnightly variation and a contribution from diurnal and higher frequency modulations. After scaling, filtering, and retaining only the first order terms, the subtidal momentum balance revealed that fortnightly waves are forced in shallow tidal rivers. It showed that terms in the subtidal momentum balance other than those representing friction and the surface elevation gradient can be neglected. The magnitude of the subtidal friction term, in turn, strongly depends on the tidal range and on river flow velocity, explaining why at a constant river discharge the surface elevation gradient features oscillations with the frequency of a spring-neap cycle. If the mean sealevel is assumed steady, this translates into fortnightly river level oscillation.

[5] The approach of *LeBlond* [1979] presumes a spectral gap between the river flow variation and fortnightly tidal

[1]Institute for Marine and Atmospheric Research Utrecht, Department of Physical Geography, Faculty of Geosciences, Utrecht University, Utrecht, Netherlands.
[2]Hydrology and Quantitative Water Management Group, Department of Environmental Sciences, Wageningen University, Wageningen, Netherlands.

0043-1397/09/2009WR008167$09.00

oscillations. That condition is usually only met in large catchments, where intramonthly river discharge variations are small, such as the St. Lawrence river that was investigated by *LeBlond* [1979].

[6] Further progress in understanding subtidal surface level variation was made by *Jay and Flinchem* [1997], who obtained an analytical expression showing how in a first order approximation the daily mean river level depends on river velocity, tidal velocity amplitude, drag coefficient, water depth, and parameters representing the rate of exponential decrease of depth and width, in upstream direction. It shows the river level to depend on the square of the river flow velocity, and on the square of the ratio of tidal velocity amplitude and river flow velocity scales. Analytical expressions were also obtained for diurnal, semidiurnal and quarterdiurnal tidal elevation amplitude.

[7] To validate the obtained expressions, *Jay and Flinchem* [1997] employed continuous wavelet transforms to decompose time series of surface elevation at several stations along the Columbia river and Estuary in unsteady low-frequent, diurnal, semidiurnal and quarterdiurnal components. They showed that analytical expressions using those decomposed time series captured the basic mechanisms of the river-tide interaction in the highly dynamic Columbia river, where discharge ranges between 2500 and over 16,000 $m^3\ s^{-1}$. *Jay and Flinchem* [1997] did not elaborate on the validation of the full expression for the daily mean river level. They emphasized that river stage varies with the square of river flow velocity, as in a uniform flow in which the effect of tides is accounted for by an elevated Chézy parameter.

[8] *Godin* [1999] provided an elaborate analysis of the friction term in the momentum balance, yielding a generic overview of periodicities involved in river-tide interactions. Crucial in his approach is the notion that the product $U|U|$ can unconditionally be approximated by two terms including the product of two constants with the first and third order terms of the nondimensionalized velocity [*Doodson*, 1924]. The constants can be calculated by expanding $U|U|$ to Chebyshev polynomials [*Dronkers*, 1964]. This allows to evaluate the subharmonics that can be expected to develop if the amplitudes of the tidal constituents at the estuarine or oceanic boundary of the tidal river are known. Also, the potential zero-frequency (permanent) steepening of the water level surface, as observed by *Godin and Martínez* [1994] in results from a numerical model, can be explained analytically from forcing conditions.

[9] *Godin* [1999] further showed that in a pragmatic approach low-passed water levels can be regressed with tidal range and river discharge, which already can yield satisfactory results. *Gallo and Vinzon* [2005] used specific cases of the overview of *Godin* [1999], to analyze how the MSf tide develops in the Amazon river.

[10] *Kukulka and Jay* [2003b] and *Kukulka and Jay* [2003a] elaborated on the work of *Jay* [1991], studying the nonlinear interactions of river flow and tides in the upriver stretches of the Columbia river at diurnal, semidiurnal, quarterdiurnal and subtidal frequencies. To do so they decomposed the friction term using the Chebyshev polynomial approach into four contributions as in the work of *Dronkers* [1964], and retained the one contribution that is dominant upriver during high flow periods, where tidal currents are weak. Assuming that the subtidal water surface gradient is constant over the investigated Columbia river reach, this allowed to obtain an analytical solution of the subtidal momentum balance, showing how water levels depend on river discharge and tidal discharge amplitude when the ratio of river discharge and tidal discharge amplitude is high. Remarkably, the obtained expression agreed well with observations, even at seaward stations close to the mouth of the Columbia river, where tidal discharge amplitudes exceed the river discharge. *Kukulka and Jay* [2003a] further pointed out that it may be necessary to account for atmospheric forcing of the subtidal water level variation, impacting especially seaward stations by about -10^{-2} m per mbar pressure increase.

[11] In this contribution a new method is presented to analyze subtidal water level dynamics in tidal rivers, and applied to the Berau river (East Kalimantan, Indonesia). The method decomposes time series of discharge and water levels into diurnal, semidiurnal, quarterdiurnal and mean flow components, using wavelet transforms as in the work of *Jay and Flinchem* [1997]. Using an approximation of the friction term provided by *Godin* [1999], a new expression for subtidal friction is derived. This new expression is used to decompose the subtidal friction into contributions from river flow, asymmetry of the tidal flow and river-tide interactions.

[12] The method proposed herein provides insight into subtidal water level dynamics generated by river and tidal flows and their interactions. This insight can be used to attribute the commonly observed rise of subtidal water levels at spring tide, with respect to neap tide, to river flow, river-tide interaction and tidal asymmetry. Based on the theoretical results as presented, a regression model can be developed relating subtidal water levels to the aforementioned contributions, aiming to predict subtidal water levels in case of peak discharges. Predicting water levels under extreme river discharge conditions will be feasible provided that the damping of diurnal and semidiurnal tides as a function of river discharge can be quantified. Such predictions are relevant for designing flood protection measures along tidal rivers.

[13] This paper continues with a description of the *tidal dynamics in the river Berau*. In section 3 a *local subtidal momentum balance* is set up for a cross section in the Berau river about 60 km from the coast, using discharge and water level data that spanned over several months. From this momentum balance equation the local subtidal water level gradient will be solved, and compared with subtidal water level differences between neighboring stations to investigate the degree in which local subtidal water level gradients represent the regional subtidal behavior. In the subsequent section, *sources of subtidal friction* are analyzed for the station where the H-ADCP is located, aiming to distinguish between contributions by river flow, by diurnal, semidiurnal and quarterdiurnal tidal velocity and by interactions of the two. The latter section is followed by a *summary and conclusions*.

2. Tidal Dynamics in the Berau River

2.1. General Characteristics

[14] Located at 2 degrees northern latitude, the Berau river is formed where two rivers join just upstream of the village Gunung Tabur, draining about 12,000 km^2 in total (Figure 1). At the downstream end, just upstream of Batu-

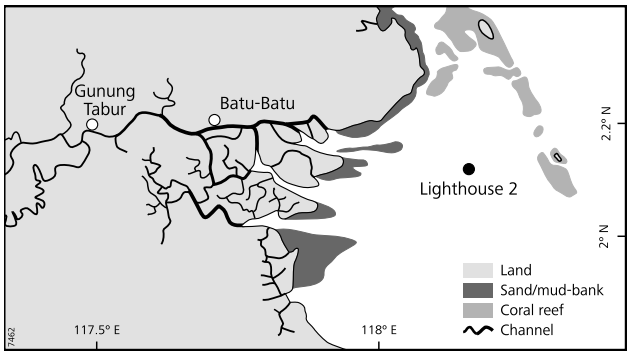

Figure 1. Topographical map of the Berau region.

Batu village, the river splits into an estuarine network. The Berau region is relatively pristine, void of constructions or dikes that may affect tides or river discharge dynamics.

[15] The planform of the Berau river, including several side channels, may be considered stable as the shorelines appear at the same position on historical maps. Figure 2 shows the bathymetry of the Berau river, based on a survey carried out in 2007. This bathymetry was obtained from sailing cross transects at least every kilometer with an echosounder and a GPS positioning system, correcting for water level variation and interpolating along the channel. The cross-sectional area increases more or less exponentially going seaward.

2.2. Discharge Data Acquisition

[16] To obtain continuous discharge estimates a 600 kHz Horizontal Acoustic Doppler Current Profiler (H-ADCP), manufactured by RD Instruments, was deployed in the Berau river at the village Gunung Tabur (Figure 1). Velocities were measured along the three beams of the H-ADCP that was mounted on a solid wooden jetty at a depth of 2.07 m below mean water level. During the deployment pitch and roll of the H-ADCP were within 1 degree, assuring that velocities were measured at nearly the same horizontal level.

[17] The velocities along the beams of the H-ADCP (u_1, u_2 and u_3), which were recorded as averages over one minute, were smoothed by a 1.5 hours moving average filter, removing the influences of turbulence and noise. This procedure was followed for 150 measuring sections of 1 m length along the middle beam (beam 3 in Figure 3). The angle in between the three acoustic beams (θ) was 25°.

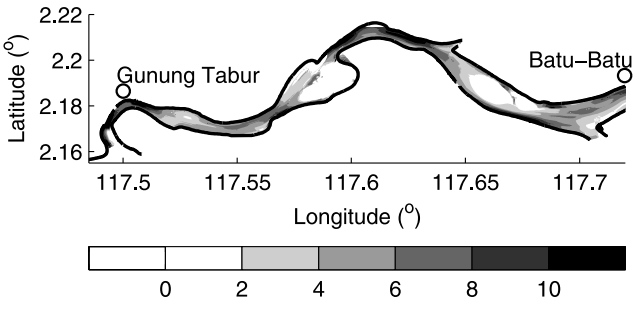

Figure 2. Bathymetry of the Berau river showing depths in m.

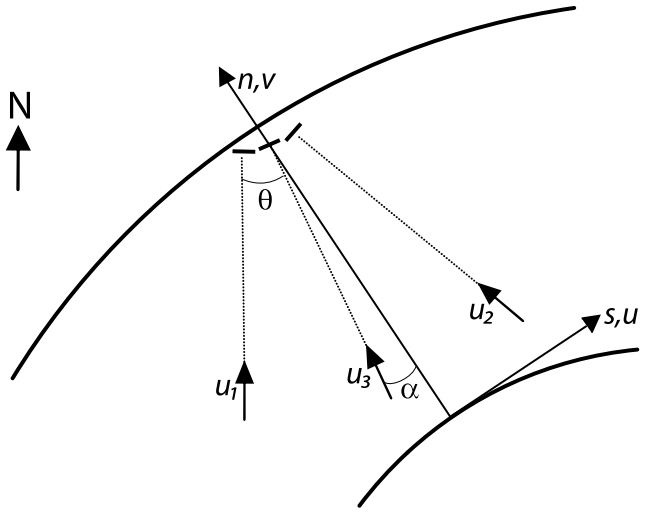

Figure 3. Definition sketch corresponding to Gunung Tabur in the Berau river (top view). The H-ADCP measures velocities along its three beams (u_1, u_2, and u_3), which are transformed to along and cross channel velocities (u and v).

Velocities along-channel and cross-channel (u and v, respectively) were calculated taking the s axis positive seaward (Figure 3), according to:

$$u = \frac{u_1 - u_2}{2\sin\theta}\cos\alpha + \frac{(u_1 + u_2)\cos\theta + u_3}{1 + 2\cos^2\theta}\sin\alpha \qquad (1)$$

$$v = \frac{-u_1 + u_2}{2\sin\theta}\sin\alpha + \frac{(u_1 + u_2)\cos\theta + u_3}{1 + 2\cos^2\theta}\cos\alpha. \qquad (2)$$

[18] The conversion of the smoothed horizontal flow velocity data to discharge was performed using the methods and calibration data described by *Hoitink et al.* [2009]. A brief description of the conversion is provided in Appendix A.

2.3. Water Level Data Acquisition and Mean Water Level Referencing

[19] During a field campaign in 2007 six months of synchronous data were collected at three stations, named Lighthouse 2, Batu-Batu, and Gunung Tabur (Figure 1). Water levels were monitored at each of the three stations from autonomous pressure gauges. The steady atmospheric conditions, characteristic at low latitudes, implied minor water level variation imposed by atmospheric pressure dynamics.

[20] Referencing the pressure transducers to a common benchmark could not be achieved in a straightforward manner, because such a benchmark is not available in this region. The difference in heights of the mean water levels at Gunung Tabur and Batu-Batu was therefore obtained indirectly. An along-channel regional momentum balance was set up for a control volume that bounds the 29 km stretch of the Berau river in between the two stations. At the upstream end, discharges were obtained continuously from the H-ADCP observations. At the downstream end, at Batu-Batu, additional discharge estimates were obtained from moving boat ADCP measurements taken over tidal

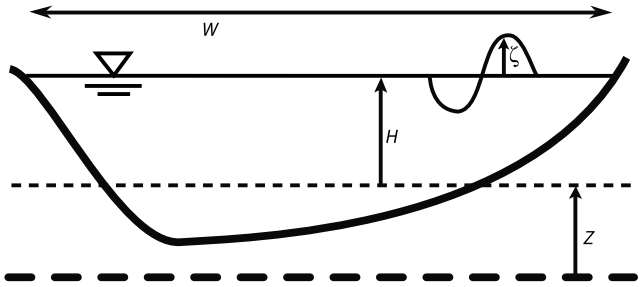

Figure 4. Channel cross section, defining the water level variation (ζ) around some width averaged depth (H) and the height of the width averaged bottom with respect to a reference level (Z).

cycles at spring tide and at neap tide. The adopted approach is described in detail in Appendix B.

[21] From the regional momentum balance the mean water level ($Z + H$ in Figure 4) at Gunung Tabur was calculated to be 0.3 m higher than at Batu-Batu, while the Chézy coefficient amounted to 40 $m^{1/2}s^{-1}$ during ebb and 45 $m^{1/2}s^{-1}$ during flood (Appendix B). The difference in mean water level between Batu-Batu and Lighthouse 2 was estimated to be 0.2 m, which was obtained by assuming a second order polynomial to fit through the mean water level profile in the tidal river and a zero mean water level gradient at sea.

2.4. Observed Water Levels

[22] Using the indirectly derived differences in mean water level between the three stations, Figure 5 (top) shows the minimum and maximum water levels per semidiurnal tidal cycle with respect to a common reference level. The tidal range at sea (station Lighthouse 2) varies from about 1 m at neap tide to about 2.5 m at spring tide, with a pronounced daily inequality. An harmonic analysis of water levels at this station shows that the tidal regime at the Berau continental shelf region is mixed, mainly semidiurnal (Table 1). Moving inland, especially the minimum water levels increase, whereas the maximum water levels rise only marginally.

[23] Figure 5 (center) displays the subtidal water levels. Moving inland from sea, subtidal water level variation is generated that co-oscillates with the tidal range. At Lighthouse 2 the variation of the subtidal water level is weak and shows no response to tidal range. The subtidal water level variation increases moving inland, and increases stronger over the tidal river stretch between Batu-Batu and Gunung Tabur than from the coastal site to Batu-Batu. At Gunung Tabur, the subtidal water level is 0.2 to 0.6 m

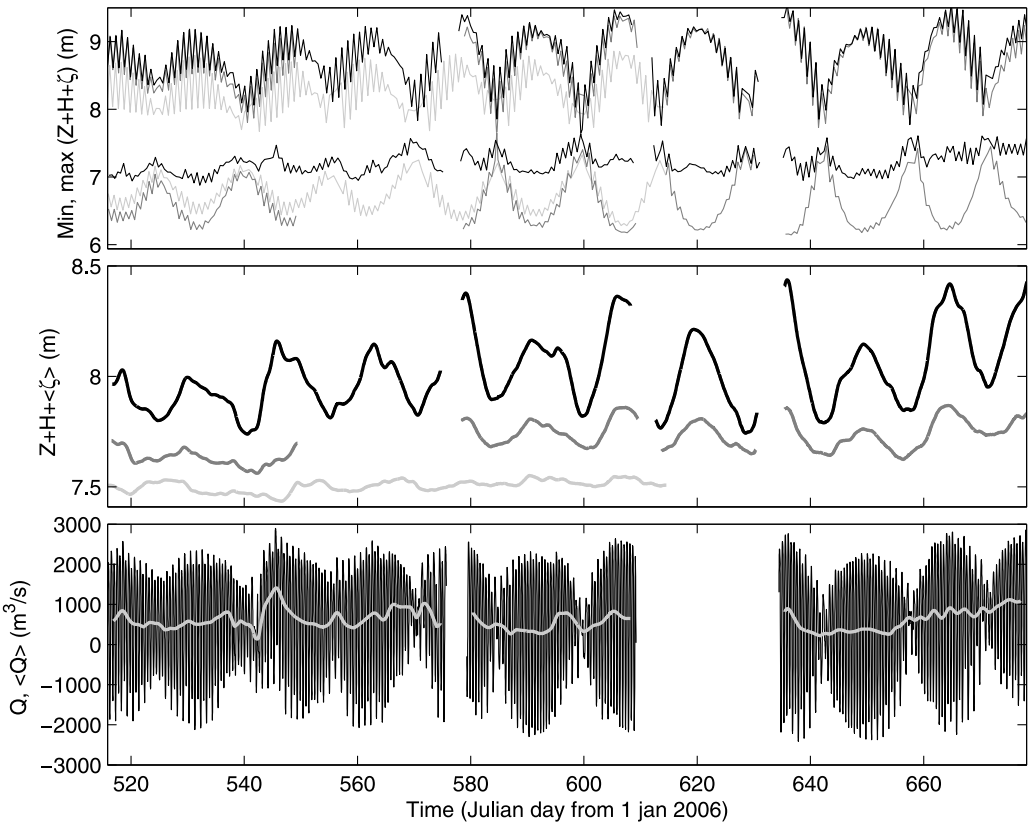

Figure 5. (top) Minimum and maximum water levels per semidiurnal tidal cycle at Lighthouse 2 (light gray), Batu-Batu (dark gray), and Gunung Tabur (black). (center) Corresponding subtidal water levels. The difference in mean water level ($H + Z$) between Batu-Batu and Gunung Tabur was resolved by setting up a momentum balance over the Berau river (Appendix B). (bottom) Discharge (black) and the subtidal discharge (fat gray) at Gunung Tabur.

Table 1. Harmonic Analysis of Water Elevation at Sea (Station Lighthouse 2) for Eight Tidal Constituents

Tidal Constituent	Amplitude (cm)	Phase (°)
M_2	70	350.57
S_2	42	220.98
N_2	10	295.26
K_2	11	243.38
K_1	17	155.61
O_1	16	12.63
P_1	7	303.79
Q_1	3	10.86

higher during spring tides than during subsequent neap tides.

[24] The higher subtidal water levels during spring tide result from the higher discharge amplitudes at spring tide with respect to neap tide (Figure 5, bottom). Higher discharge amplitudes cause an increase of the daily mean friction force. To transport the same volume of river water seaward at spring tide, an increased subtidal water level gradient is needed. Assuming that river discharge remains constant over a spring neap cycle, the variation of the subtidal water surface gradient with the tidal range causes subtidal water levels in tidal rivers to be higher at spring tide than at neap tide. Given the predominance of the main semidiurnal constituents M_2 and S_2 in the Berau river, a large portion of the subtidal variance of water levels can be attributed to MSf oscillation.

2.5. Observed Discharge

[25] Figure 5 (bottom) shows time series of discharge at Gunung Tabur. Generally, discharges at peak ebb and peak flood are similar in magnitude. The ebb period is significantly longer, accommodating the transport of river discharge. At the peak river discharges measured in the period under study, the duration of flood periods is reduced, but flood conditions were not extinguished. During the observation periods, the subtidal discharge amounted to 605 $m^3\ s^{-1}$ on average and ranged between 135 and 1412 $m^3\ s^{-1}$.

[26] The subtidal discharge variation barely features a variation at periods that coincide with those of known subharmonic tides. The correlation function between subtidal water levels at Gunung Tabur and subtidal discharges was low. Even for lagged correlation functions, the maximum correlation was low (r = 0.35 at a lag of 5 hours). This shows that the MSf discharge variation is at least an order of magnitude smaller than the river discharge. The river discharge, in turn, is shown to be highly dynamic. Local minimum values are separated from local peak river discharges by merely a few days. This suggests that for relatively small catchments like the Berau, where discharge responds rapidly to rainfall, the river discharge can be considered uncontrolled by the tidal motion, despite that a spectral frequency gap between subharmonic tidal motion and river discharge variation is absent [see *LeBlond*, 1979].

3. Local Subtidal Momentum Balance

3.1. Assumptions to be Verified

[27] Assuming absence of subtidal motions at sea, the subtidal surface height above mean sea level at any location along a tidal river can be obtained by integrating the subtidal water surface gradient from the river mouth to the specified location. Based on this consideration, local (i.e., at a river cross section) subtidal surface levels are generally assumed to co-oscillate with local subtidal surface level gradients, and subharmonic tidal oscillation of water levels is often linked directly to local variation in subtidal bottom friction [e.g., *Godin*, 1999].

[28] The degree to which this holds depends on the following two aspects. Firstly, it assumes that local and regional (i.e., over a river stretch of tens of kilometers) subtidal surface level gradients are equal. In general, this assumption bears limited validity, since subtidal surface level gradients vary along the river [*Godin and Martínez*, 1994]. Secondly, it assumes terms in the subtidal momentum balance other than the terms representing friction and the pressure gradient to be negligible. At a cross section, subtidal water surface gradients may then directly be related to flow velocities and bottom roughness.

[29] The data set described in the former section, with four months of discharge observations, allows to verify those two assumptions. From the subtidal momentum balance at Gunung Tabur the local subtidal water surface gradient can be inferred. This gradient is compared with the regional subtidal gradient obtained from neighboring water surface level gauges.

3.2. General Derivation

[30] Assuming constant water density the St. Venant equations, the governing cross section averaged local fluxes of momentum and mass, read:

$$\frac{\partial Q}{\partial t} + \frac{\partial}{\partial s}\frac{Q^2}{A} = -gA\left(\frac{\partial(Z+H+\zeta)}{\partial s} + \frac{Q|Q|}{C^2A^2(H+\zeta)}\right) \quad (3)$$

$$\frac{\partial A}{\partial t} + \frac{\partial Q}{\partial s} = 0. \quad (4)$$

where $A(s, t)$ is cross-sectional area, $Q(s, t)$ is discharge through the considered cross section, $Z(s)$ is width averaged bottom height above a reference level, $H(s)$ is mean depth, $\zeta(s, t)$ is the water level with respect to a mean level $(Z + H)$ and $C(s, t)$ is the Chézy coefficient (Figure 4). The s coordinate is taken positive seaward along the channel.

[31] Using the mass balance, the advection term can be rewritten according to:

$$\begin{aligned}\frac{\partial}{\partial s}\frac{Q^2}{A} &= -\frac{2Q}{A}\frac{\partial A}{\partial t} - \frac{Q^2}{A^2}\frac{\partial A}{\partial s} \\ &= -\frac{2Q}{A}\frac{\partial A}{\partial t} - \frac{Q^2}{A^2}\left(\frac{\partial A_m}{\partial s} + W\frac{\partial \zeta}{\partial s} + \zeta\frac{\partial W}{\partial s}\right).\end{aligned} \quad (5)$$

Herein, $W(s)$ denotes the channel width, which is considered constant in time and represents both the storage width and the flow width, and A_m is the cross-sectional area beneath mean surface level. The gradient in cross-sectional area has been split into a term representing the gradient caused by spatial changes in width and depth below the mean water level, and a temporal gradient due to differences in the water level fluctuations with respect to the mean level. Substituting the advection term in equation (3) by equation (5), rewriting $Q/A = U$ and averaging the resulting momentum balance over a diurnal tidal cycle (denoted by angular

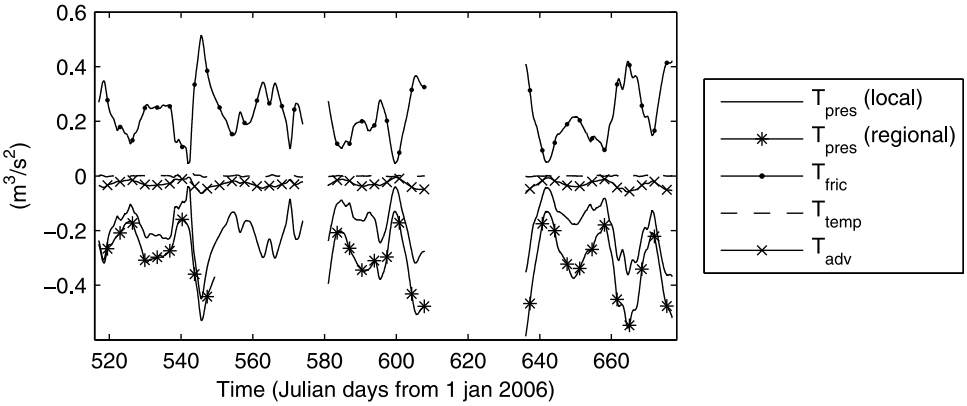

Figure 6. Terms in the subtidal local momentum balance at Gunung Tabur (equation (6)) and a regional equivalent of subtidal pressure gradient. The regional equivalent, including the difference between mean water level at Batu-Batu and Gunung Tabur (Appendix B), is for comparison with local values.

brackets), results in the following subtidal momentum balance:

$$\underbrace{\left\langle \frac{\partial Q}{\partial t} \right\rangle}_{T_{temp}} \underbrace{-\left\langle 2U\frac{\partial A}{\partial t} + U^2\left(\frac{\partial A_m}{\partial s} + W\frac{\partial \zeta}{\partial s} + \zeta\frac{\partial W}{\partial s}\right)\right\rangle}_{T_{adv}} + \underbrace{\left\langle gA\frac{\partial (Z+H+\zeta)}{\partial s}\right\rangle}_{T_{pres}} + \underbrace{\left\langle gW\frac{U|U|}{C^2}\right\rangle}_{T_{fric}} = 0. \quad (6)$$

3.3. The Subtidal Balance at Gunung Tabur

[32] To derive the local subtidal water level gradient from observed water level variations and discharge at Gunung Tabur, values of C, and $\partial A_m/\partial s$ need to be determined.

[33] The bed roughness (z_0) was adopted from the work of *Hoitink et al.* [2009], where values of z_0 were inferred during ebb and flood at Gunung Tabur from boat mounted ADCP transects (Appendix A). The cross section averaged z_0 determined over period of full ebb and over the period of full flood were 2.2 10^{-3} m and 0.4 10^{-3} m, respectively. The difference between these two roughnesses may be related to dunes that are present in part of the cross section. During ebb the flow faces the mildly sloping side of the dunes, while at flood tide the dune sides with steep slopes are exposed.

[34] The Chézy coefficient can be obtained from z_0 according to:

$$C = 5.75\sqrt{g}\ \log_{10}\frac{12R}{30z_0} \quad (7)$$

where $R \approx A/(2(H+\zeta)+W)$ is hydraulic radius [*van Rijn*, 1990]. The Chézy coefficients pertaining to the cross section at Gunung Tabur obtained accordingly amount to 56 $m^{1/2}\ s^{-1}$ for ebb tide and 70 $m^{1/2}\ s^{-1}$ for flood tide.

[35] From the bathymetry of the tidal river in the vicinity of Gunung Tabur the longitudinal gradient of the cross-sectional area, $\partial A_m/\partial s$, was established to amount to 0.2 m (see Figure 2). This fixes $\partial W/\partial s$ at 0.03, since the cross section averaged depth was constant in the vicinity of the investigated cross section.

[36] With those approximations, the local subtidal surface elevation gradient can be solved from equation (6). Figure 6 presents the variation of the four terms in the local subtidal momentum balance, confirming that the subtidal pressure term is dominantly balanced by subtidal friction. Those results are in agreement with *LeBlond* [1979] who showed that inertial effects are negligible in the subtidal balance of the upper Saint Lawrence river and with *Gallo and Vinzon* [2005], who found that subtidal friction has the largest influence on MSf surface level variations in the Amazon tidal river.

[37] The difference in Chézy coefficients between ebb and flood will have an effect on the subtidal momentum balance. It was found that the Chézy coefficient is higher during flood, compared to ebb. The drag from the bed is thus higher during ebb tide than during flood tide. If the Chézy coefficient for flood tide would have the value of the Chézy coefficient for ebb flow, typically the difference in subtidal friction between subsequent spring and neap periods remains the same. Consequently, intratidal variation of the Chézy coefficient has limited influence on subtidal water level variation.

[38] Looking in detail, Figure 6 shows that the advection term co-oscillates with the pressure term, while its magnitude is 6 to 10 times smaller. Despite that the Gunung Tabur station is a location where width variations are not particularly high, the advection term, that accounts for spatial accelerations, does play a nonnegligible role locally. The temporal acceleration term can be considered irrelevant all throughout the measurement period.

[39] Besides the local subtidal pressure gradient obtained from equation (6), Figure 6 shows the regional equivalent, which was obtained by multiplying the difference between surface elevation at Gunung Tabur and at Batu-Batu with the gravity acceleration and the cross-section at Gunung Tabur. The absolute regional subtidal pressure gradient is systematically higher, which may be attributed to a higher regional than local friction, or to the fact that the effect of spatial accelerations, captured in the advection term, vanish when a momentum balance is set up for a control volume over an increasingly larger stretch of a river.

[40] The correlation between the subtidal water level and local subtidal water surface gradient has a skill of $r^2 = 0.88$ for the case of Gunung Tabur. The present analysis suggests

that such a high correlation, which is implicitly assumed in many studies, can be partly explained from the fact that the advection term and the local pressure gradient term in the subtidal momentum balance covary.

4. Sources of Subtidal Friction

4.1. Method of Analysis

[41] *Godin* [1999] presented an elaborate algebraic development of the friction term in a momentum balance setup for tidal river applications. He describes the subharmonics, harmonics at tidal frequencies and superharmonics that result from interactions between an indefinite number of basic harmonics with arbitrary angular frequencies and phase inclinations, by substituting those in a cubic approximation of $U|U|$ in the friction term. This has yielded general insight into the redistribution of tidal energy in the frequency domain, under the influence of river flow.

[42] The present approach uses field data from a cross section in a tidal river to derive subtidal friction. The approach retains the approximation of the friction term as in the work of *Godin* [1999]. For the basic harmonics, however, a set of angular frequencies were chosen that coincide with the array of angular frequencies pertaining to a wavelet transform of the measured velocity. The set of angular frequencies was chosen such that it includes the angular frequencies of diurnal, semidiurnal and quarter diurnal tidal components, which altogether explain the vast majority of velocity variance at tidal frequencies.

[43] When a wavelet analysis is then applied to a local time series of U, the results of the algebraic development can be used to decompose subtidal variation of friction into contributions caused by the river flow, by tidal asymmetry, and by the interaction between river flow and the various tidal constituents. In the remainder of this section this new method of analysis is applied to the case of the station at Gunung Tabur.

4.2. Decomposing the Subtidal Friction

[44] The product $U|U|$ in the friction term (equation (6)) is a nonlinearity that may be approximated with the Chebyshev polynomial approach *Dronkers* [1964]. Using only the first and third order terms of the nondimensionalized velocity is sufficient to obtain an accurate approximation [*Godin*, 1991, 1999]. Adopting the latter approximation and averaging the friction term over a tidal cycle yields:

$$\frac{gW}{2\pi C^2}\int_0^{2\pi} U|U|\mathrm{d}t \approx \frac{gWU_m^2}{2\pi C^2}\int_0^{2\pi}\left(a\tilde{U}+b\tilde{U}^3\right)\mathrm{d}t \qquad (8)$$

where $\tilde{U}$ is the velocity nondimensionalized by the maximum velocity (U_m). The constants a and b take the values 0.3395 and 0.6791, respectively [*Godin*, 1999]. The constants arise from using Chebyshev polynomials to approximate $U|U|$ guaranteeing the least maximum absolute error [*Godin*, 1999].

[45] The approximation of $U|U|$ [*Godin*, 1999] was compared to the more common approximation of $U|U|$ by *Dronkers* [1964]. In the approach of *Dronkers* [1964], U is nondimensionalized by tidal velocity amplitude. The resulting approximation consists of four terms with coefficients that depend on the ratio of river flow velocity and tidal velocity amplitude. Besides terms including U and U^3 (as in equation (8)), terms including U^2 and U^4 are present. Using the approximation of $U|U|$ according to the work of *Godin* [1999], the absolute error was maximally 0.03 $m^2\ s^{-2}$ and averaged 0.02 $m^2\ s^{-2}$. The approximation as in the work of *Dronkers* [1964] gave lowest maximum absolute error when the mean river velocity and the mean spring velocity amplitude were used to nondimensionalize U. In that case, the maximum and mean absolute errors were the same as for the approximation according to the work of *Godin* [1999]. This supports the use of the more simple approach of *Godin* [1999].

[46] A set of tidal constituents within the diurnal or semidiurnal species can be lumped into a single combined harmonic, with varying amplitude and phase (equations (13) and (14) in *Hoitink et al.* [2003]). This can analogously be done for tidal constituents in the quarter diurnal species. Considering that velocity variation over a diurnal tidal cycle occurs predominantly at diurnal, semidiurnal and quarter-diurnal frequencies, *?* can be approximated according to:

$$\tilde{U} \approx \tilde{U}_0 + \tilde{U}_1\cos(\omega t+\phi_1) + \tilde{U}_2\cos(2\omega t+\phi_2) + \tilde{U}_4\cos(4\omega t+\phi_4) \qquad (9)$$

where $\tilde{U}_0$ is nondimensional subtidal velocity, $\tilde{U}_1$, $\tilde{U}_2$ and $\tilde{U}_4$ are diurnal, semidiurnal and quarterdiurnal nondimensional velocity amplitudes, respectively, ω is the angular frequency of the diurnal tide and ϕ_1, ϕ_2 and ϕ_4 are diurnal, semidiurnal and quarterdiurnal phase lags, respectively. Substituting equation (9) in equation (8) yields after elaboration:

$$\frac{U_m^2Wg}{2\pi C^2}\int_0^{2\pi}\left(a\tilde{U}+b\tilde{U}^3\right)\mathrm{d}t = \frac{U_m^2Wg}{C^2}\left(\underbrace{a\tilde{U}_0+b\tilde{U}_0^3}_{S_r}+\underbrace{\frac{3b}{2}\left(\tilde{U}_0\tilde{U}_1^2+\tilde{U}_0\tilde{U}_2^2+\tilde{U}_0\tilde{U}_4^2\right)}_{S_{rt}} + \underbrace{\frac{3b}{4}\left(\tilde{U}_1^2\tilde{U}_2\cos(2\phi_1-\phi_2)+\tilde{U}_2^2\tilde{U}_4\cos(2\phi_2-\phi_4)\right)}_{S_t}\right) \qquad (10)$$

[47] The terms indicated by S_r, S_{rt} and S_t quantify the contributions by river flow alone, river-tide interactions and tidal asymmetry to the generation of subtidal friction (respectively). The product $a\tilde{U}_0$ is the only component in the equation that is not a triple product of velocity. It potentially has the highest contribution to subtidal friction, since $\tilde{U}$ never exceeds unity.

[48] Considering that $\tilde{U}_0$ and $\tilde{U}_2$ are in general substantially larger than $\tilde{U}_1$ and $\tilde{U}_4$, equation (10) shows that S_{rt} will be dominant over S_t in many regions. Inspection of S_{rt} reveals that the relative contribution of a species is proportional to its amplitude squared. If a semidiurnal tidal wave becomes more asymmetric at a constant river discharge and energy transfer occurs to quarterdiurnal tidal oscillation, S_{rt} can be expected to increase as the $\tilde{U}_4$ generally increases more than that $\tilde{U}_2$ decreases. The phases of the tidal species

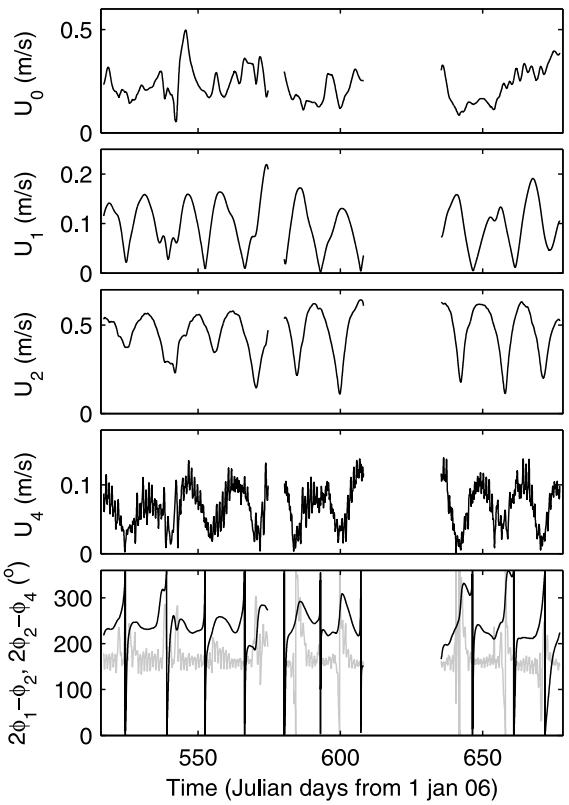

Figure 7. (top) Subtidal velocity at Gunung Tabur. (center) Diurnal, semidiurnal, and quarterdiurnal velocity amplitudes at Gunung Tabur. (bottom) Phase differences between diurnal and semidiurnal tidal species (black) and between semidiurnal and quarterdiurnal tidal species (gray).

are irrelevant to subtidal friction resulting from the river-tide interaction, because they do not appear in S_{rt}.

[49] In natural tidal rivers, velocity amplitudes remain largely constant along the channel, as the energy losses by friction are compensated for by channel convergence [*Savenije*, 2005]. River flow velocity decreases in downstream direction as a result of the increase of channel width. The contribution of S_{rt} to subtidal friction thus decreases when going downstream.

[50] The magnitude of S_t is very much dependent on the relative phases of the different tidal constituents. Whereas contributions to subtidal friction due to river flow and river-tide interactions are always positive, S_t can either be positive or negative, depending on the phases of tidal constituents. The contribution of S_t is absent when $2\phi_1 - \phi_2 = 2\phi_2 - \phi_4 = 0$, and is maximal when both $2\phi_1 - \phi_2$ and $2\phi_2 - \phi_4$ equal $\pm 180°$. The absolute contribution of S_t is usually highest at spring tide and lowest at neap tide.

[51] In a shallow channel, where semidiurnal tidal energy is transferred to quarterdiurnal tidal energy, the phase difference between semidiurnal and quarterdiurnal species usually approaches 180° [*Friedrichs and Aubrey*, 1988]. Phase differences between the diurnal and semidiurnal constituents are mainly dependent on phase differences at the estuarine or coastal boundary of the tidal river. It would be interesting to investigate tidal rivers in mixed diurnal-semidiurnal tidal regimes, where $\tilde{U}_1$ and $\tilde{U}_2$ are equal in magnitude. If the tidal energy is spread over $\tilde{U}_1$ and $\tilde{U}_2$ rather than concentrated in one of the two species, S_t may be expected to be larger relative to S_{rt}.

4.3. Wavelet Analysis of Observations

[52] In contrast to harmonic analysis, continuous wavelet theory is well suited for analyzing river tides, as it does not assume stationarity of a time series [*Jay and Flinchem*, 1997; *Flinchem and Jay*, 2000]. In terms of the variables in equation (9), U_0 is nonstationary and acts to continuously alter the (dimensional) amplitudes U_1, U_2 and U_4 as well as the phases ϕ_1, ϕ_2 and ϕ_4.

[53] By applying a wavelet transform to a time series of either $\tilde{U}$ or ζ, a wavelet power spectrum and a phase spectrum results, from which those amplitudes and phases can readily be derived. The cross section averaged velocity U and the water levels ζ at Gunung Tabur were subjected to a continuous wavelet transform using the Morlet wavelet function, adopting the methods described by *Torrence and Compo* [1998]. In wavelet analysis, one is limited to an array of angular frequencies that can be written as fractional powers of two:

$$\omega_j = \omega_0 2^{-j\,\delta j},\ j = 0, 1, 2, \ldots, J \tag{11}$$

$$J = \delta j^{-1} \log_2 (N \delta t\, \omega_0) \tag{12}$$

where δt is the time spacing in the data series, $N\ \delta t$ is window length that a wavelet covers, ω_0 is the highest frequency resolved, J determines the lowest frequency and δj is a parameter determining the frequency resolution. Here ω_0 is chosen as the angular frequency of the M_4 tide and the window length $N\ \delta t$ is taken as the period of the M_1 carrier wave [see *Woodworth et al.*, 2005; *Hoitink et al.*, 2006]. The minimum value for δj depends on the width in spectral space of the wavelet function, and is about 0.5 for a Morlet wavelet [*Torrence and Compo*, 1998], as adopted here. Setting $\delta j = 1$ results in a frequency array that already would include diurnal, semidiurnal and quarterdiurnal species, but raising the frequency resolution provides robustness against data noise [*Flinchem and Jay*, 2000].

[54] Time series of U_0, U_1, U_2 and U_4 based on wavelet transformation of U are shown in Figure 7. The semidiurnal species dominates the velocity signal, and features more variation in amplitude minimums than amplitude maximums, which remain in between 0.5 and 0.6 ms^{-1}. Variation of the neap tide values of U_2 cannot be readily related to fluctuation of the river flow or to the other tidal species. Values of U_4 co-oscillate with U_2, and $2\phi_2 - \phi_4$ typically takes a value of 180°, suggesting that asymmetry of the semidiurnal tides, captured in U_4 generation, may cause relatively large subtidal friction (equation (10)). The phase difference $2\phi_1 - \phi_2$ is close to 230°, suggesting that the contribution to subtidal friction from the interaction between diurnal and semidiurnal tides is usually small with respect to the interaction of semidiurnal and quarterdiurnal tides.

[55] Figure 8 shows the wavelet transforms of water level variations at Lighthouse 2, Batu-Batu and Gunung Tabur, where water level amplitudes of the diurnal, semidiurnal and quarter diurnal tidal species are denoted by ζ_1, ζ_2 and ζ_4 (respectively). In the estuarine branches in between Lighthouse 2 and Batu-Batu the diurnal tidal species remain invariant, whereas the semidiurnal tidal species amplify, and

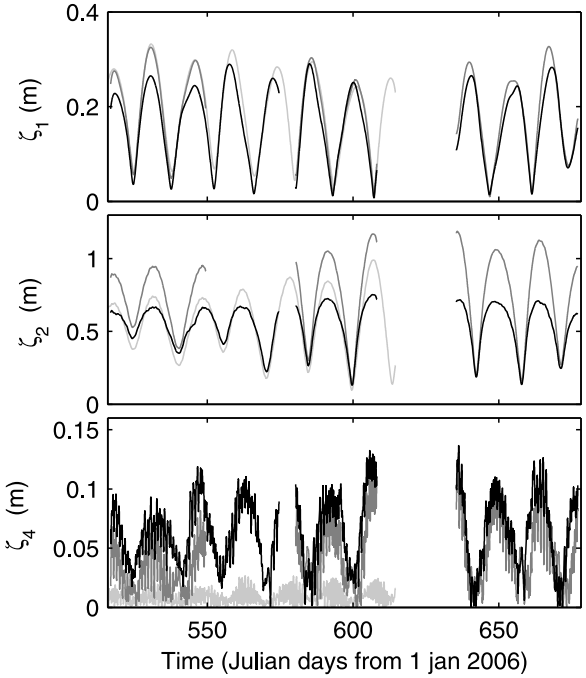

Figure 8. Diurnal, semidiurnal, and quarterdiurnal water level amplitudes, respectively, resulting from wavelet analysis at Lighthouse 2 (light gray), Batu-Batu (dark gray), and Gunung Tabur (black).

quarter diurnal tidal energy is generated. In the river section between Batu-Batu and Gunung Tabur both the diurnal and the semidiurnal species attenuate by friction whereas the quarterdiurnal species amplify weakly. The development of ζ_2 in this section illustrates how friction acts to reduce the variation in spring tide maximums of ζ_2 in upriver direction, whereas neap tide minimums of ζ_2 can be just as variable at an inland location as near the coast.

4.4. Regression Model for $\langle\zeta\rangle$

[56] Using the wavelet transformation of U at Gunung Tabur, the contributions of S_r, S_{rt} and S_t to subtidal friction are shown Figure 9 (top). Clearly, the river flow has a major influence on subtidal friction at Gunung Tabur, and exceeds the contribution by river-tide interaction even when river flow is significantly below the semidiurnal tidal velocity amplitude. The interaction of the quarterdiurnal and the semidiurnal species, resulting in longer ebb periods where the peak is reduced and shorter but more intense flood periods, results in a minor negative contribution to subtidal friction.

[57] Having established the contributions of S_r, S_{rt} and S_t to the local subtidal friction balance at Gunung Tabur, it is of interest to investigate how well $\langle\zeta\rangle$ can be predicted from those terms, revealing the extent to which regional subtidal water level dynamics responds to local subtidal friction variation.

[58] Table 2 presents the skill (r^2) and error variance (ϵ) for single, dual and triple linear regression models for $\langle\zeta\rangle$. Rigorously fitting $\langle\zeta\rangle$ with either $S_t + S_{rt} + S_t$ or with S_r results in surprisingly low skills of 0.43 and 0.2, respectively. The best single linear fit is obtained using S_{rt}, resulting in a skill of 0.74, whereas the fit with the tidal asymmetry term S_t is also quite high ($r^2 = 0.64$). Employing a dual or triple linear regression model does not raise the skill considerably, nor does it reduce the error variance significantly.

[59] The poor correlation between variation in S_r and $\langle\zeta\rangle$ can be explained by the decrease of U_0 in seaward direction, caused by the exponential increase of cross-sectional area. At Batu-Batu, U_0 has already decreased by about 70% relative to Gunung Tabur, whereas U_1 and U_2 slightly increase.

[60] The relative importance of S_{rt} and S_t to subtidal friction will further increase moving seaward. The correlation between S_t and $\langle\zeta\rangle$ is high, while the contribution of S_t to subtidal friction is of minor importance at Gunung Tabur (Figure 9, top). The high correlation is caused by the fact that, although U_0 does not appear in S_t, it does have a control over that term since it modulates the tidal velocity amplitudes *Horrevoets et al.* [2004]. This river control over U_1, U_2 and U_4 is also relevant to the magnitude of S_{rt}.

[61] The former regression analysis may be compared to results obtained by adopting the approaches of *Godin* [1999] and *Kukulka and Jay* [2003a]. *Godin* [1999] regressed the subtidal water level variation at Grondines with river discharge and tidal range. A similar regression is performed for the case of Gunung Tabur using the river discharge (Q_r) and semidiurnal tidal amplitude at Gunung Tabur, resulting in a skill of 0.64 (Table 2). *Kukulka and Jay* [2003a] used the following regression relation:

$$\langle\zeta\rangle = c_1 Q_r^{2/3} + c_2 \frac{R_0^2}{Q_r^{4/3}} + c_3 \frac{\partial p_{atm}}{\partial s} + c_4 \qquad (13)$$

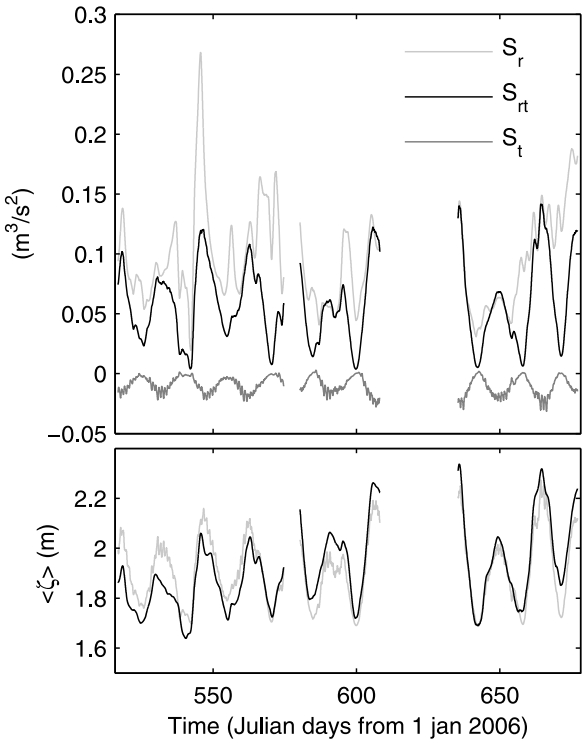

Figure 9. (top) Contributions to subtidal friction at Gunung Tabur (equation (10)) from river solely (S_r), the interaction of tides and river flow (S_{rt}), and interactions of tidal species (S_t). (bottom) Comparison between $\langle\zeta\rangle$ variation and predictions of $\langle\zeta\rangle$ from S_{rt}, using results of a linear regression (gray). See also Table 2.

Table 2. Single, Dual, and Triple Linear Regressions Models for $\langle\zeta\rangle$

Regression Type	$\langle\zeta\rangle$ =	r^2	ϵ (m^2)
Single	1.6 (S_t + S_{rt} + S_t)	0.43	0.0142
Single	1.7 S_r	0.20	0.0198
Single	−17 S_t	0.64	0.0088
Single (plotted)	4.0 S_{rt}	0.74	0.0065
Dual	3.0 S_{rt} −5.7 S_t	0.75	0.0061
Dual [*Godin*, 1999]	2.8 10^{-4} Q_r +0.76 ζ_2	0.64	0.0061
Dual [*Kukulka and Jay*, 2003a]	5.6 10^{-3} $Q_r^{2/3}$ +1.6 10^3 $\zeta_2^2/Q_r^{4/3}$	0.62	0.0061
Triple	0.10 S_r +2.8 S_{rt} −6.3 S_t	0.76	0.0060

where R_0 is tidal range at the estuary entrance, p_{atm} is atmospheric pressure and c_1, c_2, c_3 and c_4 are regression coefficients. Applying this regression model to the Berau river, using the semidiurnal tidal amplitude at Lighthouse 2 for the tidal range at the estuary entrance and neglecting the atmospheric pressure gradient, results in a skill of 0.62.

[62] The Figure 9 (bottom) compares variation of $\langle\zeta\rangle$ at Gunung Tabur from measurements and from the regression model $\langle\zeta\rangle = 4S_{rt}$. Although U_0 was highest on Julian day 545, $\langle\zeta\rangle$ was lower than two spring-neap periods later, when U_2 was similar and U_0 had decreased considerably. The additional damping of the semidiurnal and diurnal tides apparently had a stronger effect on reducing S_{rt} than the raise of both S_r and S_{rt} due to increased U_0, which may relate to the fact that U_1, U_2 and U_4 appear quadratically in S_{rt}.

[63] The results obtained above potentially can be used for a stochastic analysis of extreme water levels at a river station. River discharge and the ratio of velocity amplitudes of tidal species at a river site and at the coastal boundary can be expected to correlate well [*Jay and Flinchem*, 1997]. Such correlations could not be established for the case of the Berau river, because coastal currents were not monitored continuously and the discharge time series probably need to be longer than four months to obtain statistically significant regression coefficients. The data series presented herein included merely a single high discharge event that had a clear effect on the tidal velocity amplitudes. If long-term data on coastal currents and discharge at a river site are available, and river site values of U_1, U_2 and U_4 can be estimated from that data, then the results of the regression between $\langle\zeta\rangle$ and S_{rt} can be used to predict changes of $\langle\zeta\rangle$ in response to extreme river discharges.

5. Summary and Conclusion

[64] A new method was introduced to analyze subtidal water level variation at a station in a tidal river where discharge and water levels are observed continuously over periods of months. It was verified that in the subtidal momentum balance for this station the water level gradient term is dominantly balanced by friction. In the subtidal friction $U|U|$ was approximated with a polynomial expression, including merely the first and third order terms of the nondimensionalized velocity [*Godin*, 1999]. The observed flow velocity was decomposed using wavelet theory, where the resolved array of angular frequencies was chosen such that the diurnal species, semidiurnal species and quarter-diurnal species of the tides are well represented. The river contribution to variation of flow velocity is represented by a zero-frequency harmonic. The results of the wavelet transformation can be used to obtain time series of S_r, S_{rt} and S_t, representing the contributions to local subtidal friction of river flow, river-tide interactions and interactions between tidal species, respectively.

[65] Several regression models were evaluated using data from the Berau river (East Kalimantan, Indonesia), aiming to investigate how well subtidal water level ($\langle\zeta\rangle$) can be predicted from S_r, S_{rt} and S_t. A straightforward approach of regressing $\langle\zeta\rangle$ with $S_r + S_{rt} + S_t$ yielded a surprisingly low correlation ($r^2 = 0.43$). The highest correlation for a single regression was obtained when regressing $\langle\zeta\rangle$ with S_{rt} ($r^2 = 0.74$). Hence the river-tide interaction component in the local subtidal friction represents the generation of variation in $\langle\zeta\rangle$ along the river reach, in between the coastal boundary and the measurement station, best.

[66] It is foreseen that in case of sufficient river discharge variation during a monitoring period, ratios of tidal amplitudes at a station to corresponding tidal amplitudes near the coast can be related to river discharge [*Jay and Flinchem*, 1997]. If such relations can be obtained, then the decrease of diurnal, semidiurnal and quarter diurnal tidal velocity amplitudes under peak river discharges can be estimated, and a correlation model for the prediction of $\langle\zeta\rangle$ from S_{rt} can be used to estimate the value of $\langle\zeta\rangle$ under peak river discharge conditions. It is expected that such an approach holds well in most tidal river environments. Only special conditions of pronounced tidal asymmetry, caused either by overtide generation or by interaction between astronomical constituents, can theoretically result in a relatively large contribution of S_t.

Appendix A: Deriving Discharge From H-ADCP Derived Flow Velocity Profiles

[67] To convert horizontal velocity profiles inferred from H-ADCP measurements into discharge, a semideterministic, semistochastic method is adopted, using the methods and calibration parameters described by *Hoitink et al.* [2009]. In this appendix, a brief summary of the method is presented. In the deterministic part of the method, the specific discharge q is obtained from single depth H-ADCP data by relying on the law of the wall:

$$\frac{u(z)}{u_*} = \frac{1}{\kappa}\ln\left(\frac{z+h}{z_0}\right) \tag{A1}$$

where h is local water depth, z is an upward pointing vertical coordinate that has its origin at the water surface, u_* is the shear velocity, κ is the Von Karman constant and z_0 is the bottom roughness length. Velocity profiles were

shown to satisfy equation (A1) up to the surface, even during slack water. Provided that the bed roughness z_0 is known, the specific discharge q can be obtained from u according to:

$$q = \frac{\ln\left(\frac{h+\zeta}{z_0 \mathrm{e}}\right)}{\ln\left(\frac{\sigma(h+\zeta)}{z_0}\right)} u(\sigma)h. \tag{A2}$$

where σ is the relative height defined by:

$$\sigma = \frac{z+h}{h+\zeta} \tag{A3}$$

[68] Cross-river profiles of the bottom roughness length z_0 were inferred from 172 moving boat ADCP transect measurements, using the following procedure. The measured velocity profiles along a transect were interpolated on a (σ, n)-grid, with 20 σ layers and a 5 m cell length in the n-direction. To remove the influence of turbulence, noise and error in the positioning, time series of $u(\sigma, n)$ were smoothed according to the methods of *Schlax and Chelton* [1992], using a turnover period of 1.5 hours. Values of z_0 are considered to depend only on the direction of the flow with respect to the roughness elements (i.e., on ebb and flood) and hence not on the flow magnitude [e.g., *Cheng et al.*, 1999]. For every 5 m section across the transect, a z_0 was determined for full ebb flow and for full flood flow. The profiles of $z_0(n)$ were then averaged geometrically over the cross section.

[69] In the subsequent part of the method, Q is related to q using the following stochastic model:

$$Q(t) = f_a(n) W q(n, t + t_r(n)) \tag{A4}$$

where W is the channel width at the mean level, $f_a(n)$ denotes an amplification factor that is assumed to be constant in time and t_r accounts for the time lag between variation in q and Q. Based on an analysis of the relative moment in time of the occurrence of slack water across the transect, the following empirical function is proposed:

$$t_r = c_1 \sin\left(\frac{n\pi}{W}\right)^{c_2} + c_3 \tag{A5}$$

where the coefficients c_1, c_2 and c_3 were obtained from regression. Velocity variation in the central part of the transect lagged behind variation near the shores by about 20 minutes. After calculating Q using conventional methods [*Muste et al.*, 2004], the amplification factors were determined from the best fit linear line through scatterplots of Q versus $Wq(n, t + t_r(n))$.

Appendix B: Regional Intratidal Momentum Balance

[70] In this appendix the difference in reference height between two stations in a tidal river is derived by setting up a regional intratidal momentum balance over the river stretch between the two stations. With this reference height difference, the mean water surface and bottom gradient over the river stretch can be determined.

[71] The regional balance is set up for the control volume covering the longitudinal stretch between Batu-Butu and Gunung Tabur with length L (about 29 km). Equation (3) is averaged over this length, yielding:

$$\frac{1}{L}\int_0^L \left(\frac{\partial UA}{\partial t} + \frac{\partial U^2 A}{\partial s} + gA\frac{\partial(Z+H+\zeta)}{\partial s} + gW\frac{U|U|}{C^2}\right)\mathrm{d}s = 0 \tag{B1}$$

where lateral inflow and density gradients are assumed to be negligible. At the downstream end of the transect between Batu-Batu and Gunung Tabur (denoted by subscripts $_B$ and $_G$, respectively), the longitudinal density gradients give rise to water surface gradients of merely $1 \cdot 10^{-6}$ at most. The cross-sectional area $A = W(H + \zeta)$ can be elaborated as follows. The width may be assumed to increase exponentially going seaward:

$$W = W_G \mathrm{e}^{\gamma s} \tag{B2}$$

Fitting this function to measured widths of the Berau river yields $\gamma = 4 \cdot 10^{-5}$. In a first order approximation, velocity (U), the bottom height above the reference level (Z) and the mean total depth ($H + \zeta$) may be assumed to vary linearly over a 29 km reach of a tidal river as the one under study. Substituting for A, the term in equation (B1) can be elaborated to yield for the temporal acceleration term:

$$\begin{aligned}\frac{1}{L}\int_0^L \frac{\partial(UA)}{\partial t}\mathrm{d}s = \frac{1}{L}\frac{\partial}{\partial t}\Bigg(&\frac{U_G(H_G+\zeta_G)(W_B-W_G)}{\gamma} \\ &+ (U_G(H_B - 2H_G + \zeta_B - 2\zeta_G) \\ &+ U_B(H_G+\zeta_G)) \cdot \frac{W_B(\gamma L - 1) + W_G}{L\gamma^2} \\ &+ (U_B - U_G)(H_B - H_G + \zeta_B - \zeta_G) \\ &\cdot \frac{W_B(\gamma L(\gamma L - 2) + 2) - 2}{L^2\gamma^3}\Bigg),\end{aligned} \tag{B3}$$

for the advection term:

$$\begin{aligned}\frac{1}{L}\int_0^L \frac{\partial(U^2A)}{\partial s}\mathrm{d}s = \frac{1}{L}\Big(&U_G^2 W_B(H_B+\zeta_B) - U_G^2 W_G(H_G+\zeta_G) \\ &+ 2W_B U_G(U_B - U_G)(H_B+\zeta_B) \\ &+ W_B(U_B - U_G)^2(H_B+\zeta_B)\Big),\end{aligned} \tag{B4}$$

for the pressure term:

$$\begin{aligned}\frac{1}{L}\int_0^L gA\frac{\partial(Z+H+\zeta)}{\partial s}\mathrm{d}s = g\frac{Z_B - Z_G + H_B - H_G + \zeta_B - \zeta_G}{L^2} \\ \cdot \Bigg((H_G+\zeta_G)\frac{W_B - W_G}{\gamma} \\ + (H_B - H_G + \zeta_B - \zeta_G) \\ \cdot \frac{W_B(\gamma L - 1) + W_G}{\gamma^2 L}\Bigg),\end{aligned} \tag{B5}$$

and for the friction term:

$$\frac{1}{L}\int_0^L gW\frac{U|U|}{C^2}\mathrm{d}s = \frac{g\,\mathrm{sign}(U)}{C^2}\left(\frac{U_G^2(W_B-W_G)}{\gamma} + \frac{2(U_B-U_G)U_G}{L}\frac{W_B(\gamma L-1)+W_G}{\gamma^2} + \frac{(U_B-U_G)^2}{L^2}\frac{W_B(\gamma L(\gamma L-2)+2)-2W_G}{\gamma^3}\right). \quad \text{(B6)}$$

[72] At Gunung Tabur, $H + \zeta$ and U were available from H-ADCP measurements. Close to Batu-Batu, discharge was determined using the methods described by *Muste et al.* [2004] for two periods of 12.5 hours, covering a tidal cycle at neap tide and one at spring tide. With the obtained water level variation at Batu-Batu and the measured bathymetry, the roughness (C) and the difference in reference height between the two stations ($Z_B - Z_G$) are the only unknowns in the equations.

[73] Assuming that the Chézy coefficient is constant during ebb and during flood, there are three unknowns to be solved. Those constants can be determined with the highest accuracy using data corresponding to peak flow conditions during both spring and neap tides. From the two peak ebb flows at spring and at neap tide, the constant $Z_B - Z_G$ and the ebb Chézy coefficient were calculated. It was confirmed that using this $Z_B - Z_G$ the resulting Chézy coefficients during peak flood flows for both spring and neap tide were constant, supporting the $Z_B - Z_G$ result.

[74] **Acknowledgments.** This study was supported by grant WT 77-203 of WOTRO Science for Global Development, a division of the Netherlands Organisation of Scientific Research (NWO). M.C.G. van Maarseveen (Utrecht University) is acknowledged for preparing and maintaining the instruments and his technical assistance. We thank A. Tarya (Utrecht University) and a number of students from Wageningen University and Utrecht University who assisted during the field campaigns. Wavelet software was provided by C. Torrence and G. Compo and is available at http://paos.colorado.edu/research/wavelets/. We thank three anonymous reviewers for their comments and suggestions.

References

Cheng, R. T., C. Ling, J. W. Gartner, and P. F. Wang (1999), Estimates of bottom roughness length and bottom shear stress in south San Francisco bay, California, *J. Geophys. Res.*, *104*(C4), 7715–7728.

Doodson, A. T. (1924), Perturbations of harmonic tidal constants, *Proc. R. Soc., Ser. A*, *106*(739), 513–526.

Dronkers, J. J. (1964), *Tidal Computations in Rivers and Coastal Waters*, North-Holland, Amsterdam.

Flinchem, E. P., and D. A. Jay (2000), An introduction to wavelet transform tidal analysis methods, *Estuarine Coastal Shelf Sci.*, *51*, 177–200.

Friedrichs, C. T., and D. G. Aubrey (1988), Non-linear tidal distortion in shallow well-mixed estuaries: A synthesis, *Estuarine Coastal Shelf Sci.*, *27*, 521–545.

Gallo, M. N., and S. B. Vinzon (2005), Generation of overtides and compound tides in Amazon estuary, *Ocean Dyn.*, *55*, 441–448, doi:10.1007/s10236-005-0003-8.

Godin, G. (1991), Frictional effects in river tides, chap. 19, in *Tidal Hydrodynamics*, pp. 379–402, Wiley, Hoboken, N. J.

Godin, G. (1999), The propagation of tides up rivers with special considerations on the upper Saint Lawrence river, *Estuarine Coastal Shelf Sci.*, *48*, 307–324.

Godin, G., and A. Martínez (1994), Numerical experiments to investigate the effects of quadratic friction on the propagation of tides in a channel, *Cont. Shelf Res.*, *14*(7/8), 723–748.

Hoitink, A. J. F., P. Hoekstra, and D. S. van Maren (2003), Flow asymmetry associated with astronomical tides: Implications for the residual transport of sediment, *J. Geophys. Res.*, *108*(C10), 3315, doi:10.1029/2002JC001539.

Hoitink, A. J. F., P. Hoekstra, and D. S. van Maren (2006), Comment on "On the role of diurnal tides in contributing to asymmetries in tidal probability distribution functions in areas of predominantly semi-diurnal tide" edited by P. L. Woodworth et. al., [Estuarine, Coastal and Shelf Science 64 (2005) 235–240], *Estuarine Coastal Shelf Sci.*, *67*, 340–341, doi:10.1016/j.ecss.2005.10.008.

Hoitink, A. J. F., F. A. Buschman, and B. Vermeulen (2009), Continuous measurements of discharge from a horizontal acoustic Doppler current profiler in a tidal river, *Water Resour. Res.*, doi:10.1029/2009WR007791, in press.

Horrevoets, A. C., H. H. G. Savenije, J. N. Schuurman, and S. Graas (2004), The influence of river discharge on tidal damping in alluvial estuaries, *J. Hydrol.*, *294*, 213–228, doi:10.1016/j.jhydrol.2004.02.012.

Jay, D. A. (1991), Green's law revisited: Tidal long-wave propagation in channels with strong topography, *J. Geophys. Res.*, *96*(C11), 20,585–20,598.

Jay, D. A., and E. P. Flinchem (1997), Interaction of fluctuating river flow with a barotropic tide: A demonstration of wavelet tidal analysis methods, *J. Geophys. Res.*, *102*(C3), 5705–5720.

Kukulka, T., and D. Jay (2003a), Impacts of Columbia river discharge on salmonid habitat: 2. Changes in shallow-water habitat, *J. Geophys. Res.*, *108*(C9), 3294, doi:10.1029/2003JC001829.

Kukulka, T., and D. A. Jay (2003b), Impacts of Columbia river discharge on salmonid habitat: 1. A nonstationary fluvial tide model, *J. Geophys. Res.*, *108*(C9), 3293, doi:10.1029/2002JC001382.

LeBlond, P. H. (1978), On tidal propagation in shallow rivers, *J. Geophys. Res.*, *83*(C9), 4717–4721.

LeBlond, P. H. (1979), Forced fortnightly tides in shallow waters, *Atmos.-Ocean*, *17*(3), 253–264.

Le Coz, J., G. Pierrefeu, and A. Paquier (2008), Evaluation of river discharges monitored by a fixed side-looking Doppler profiler, *Water Resour. Res.*, *44*, W00D09, doi:10.1029/2008WR006967.

Muste, M., K. Yu, and M. Spasojevic (2004), Practical aspects of ADCP data use for quantification of mean river flow characteristics: Part 1. Moving-vessel measurements, *Flow Meas. Instrum.*, *15*, 1–16, doi:10.1016/j.flowmeasinst.2003.09.001.

Nihei, Y., and A. Kimizu (2008), A new monitoring system for river discharge with horizontal acoustic Doppler current profiler measurements and river flow simulation, *Water Resour. Res.*, *44*, W00D20, doi:10.1029/2008WR006970.

Savenije, H. H. G. (2005), *Salinity and Tides in Alluvial Estuaries*, Elsevier, Amsterdam.

Schlax, M. G., and D. B. Chelton (1992), Frequency domain diagnostics for linear smoothers, *J. Am. Stat. Assoc.*, *87*(420), 1070–1081.

Torrence, C., and G. P. Compo (1998), A practical guide to wavelet analysis, *Bull. Am. Meteorol. Soc.*, *79*(1), 61–78.

van Rijn, L. C. (1990), *Principles of Fluid Flow and Surface Waves in Rivers, Estuaries, Seas and Oceans*, Aqua Publ., Amsterdam.

Woodworth, P. L., D. L. Blackman, D. T. Pugh, and J. M. Vassie (2005), On the role of diurnal tides in contributing to asymmetries in tidal probability distribution functions in areas of predominantly semi-diurnal tide, *Estuarine Coastal Shelf Sci.*, *64*, 235–240, doi:10.1016/j.ecss.2005.02.014.

F. A. Buschman, P. Hoekstra, and M. van der Vegt, Institute for Marine and Atmospheric Research Utrecht, Department of Physical Geography, Faculty of Geosciences, Utrecht University, Heidelberglaan 2, P.O. Box 80.115, 3508 TC Utrecht, Netherlands. (frans.buschman@gmail.com; p.hoekstra@geo.uu.nl; m.vandervegt@geo.uu.nl)

A. J. F. Hoitink, Hydrology and Quantitative Water Management Group, Department of Environmental Sciences, Wageningen University, Droevendaalsesteeg 4, P.O. Box 47, 6700 AA Wageningen, Netherlands. (ton.hoitink@wur.nl; t.hoitink@geo.uu.nl)